Applied Physics Letters

RESEARCH ARTICLE | OCTOBER 19 2023

Electrically driven nanoantenna metasurface for coherent thermal emission

Lin Jing ; Xiu Liu; Hakan Salihoglu ; Xiao Luo ; Hyeong Seok Yun ; Zexiao Wang ; Sheng Shen

Appl. Phys. Lett. 123, 161703 (2023)
https://doi.org/10.1063/5.0165104

AIP Publishing

Applied Physics Letters ARTICLE pubs.aip.org/aip/apl

Electrically driven nanoantenna metasurface for coherent thermal emission

Cite as: Appl. Phys. Lett. **123**, 161703 (2023); doi: 10.1063/5.0165104
Submitted: 14 July 2023 · Accepted: 11 October 2023 ·
Published Online: 19 October 2023

Lin Jing, Xiu Liu, Hakan Salihoglu, Xiao Luo, Hyeong Seok Yun, Zexiao Wang, and Sheng Shen[a)]

AFFILIATIONS

Department of Mechanical Engineering, Carnegie Mellon University, Pittsburgh, Pennsylvania 15213, USA

[a)]Author to whom correspondence should be addressed: sshen1@cmu.edu

ABSTRACT

Nanoantennas and their arrays (metasurfaces) provide a versatile platform for controlling the coherence of thermal emission. Conventional designs rely on global heating, which impedes emission efficiency and on-chip integration. In this work, we propose an electrically driven metasurface composed of a Yagi-Uda nanoantenna array interconnected by S-shaped electrode wires, which enables the concurrent manipulation of thermal emission spectrally and directionally. A direct simulation approach based on the Wiener-chaos expansion method is employed for quantitative analysis. Our metasurface device exhibits a narrowband emission with high directivity, which is one order higher than that of a single nanorod antenna case. The modeling framework established in this work opens a promising route for realizing coherent mid-infrared emission by metasurfaces.

The capability of controlling thermal emission has enabled myriads of applications, such as infrared imaging,[1] biochemical sensing,[2,3] radiative cooling,[4] thermal circuits,[5] and energy harvesting.[6,7] However, intrinsic incoherence of thermal emission, for example, thermal radiation from incandescent tungsten filaments, imposes significant limitations on the efficiency, selectivity, and sensitivity in these applications. To achieve coherent emission, i.e., monochromatic emission with high directionality, metasurfaces[8–10] and metamaterials[11–14] provide a promising platform for tailoring the emission spectrally[15–18] or directionally.[19–21] Here, narrow spectrum is usually a measure of the temporal coherence of a thermal source, and directivity indicates the spatial transverse coherence.[22] To date, nanoresonator arrays[15,18,23,24] and plasmonic metasurfaces[25] have demonstrated narrowband nearly perfect thermal emission, while grating structures[19,20] and nanoantennas[26] yield narrow angular emission.

Owing to the highly efficient beaming effect for electromagnetic waves,[27,28] the Yagi-Uda antenna (YUA) has been adopted from its original application in radio waves to other frequency ranges, especially for visible light,[29–36] due to the advancement of nanofabrication technologies. However, in the infrared regime, thermally exciting a YUA with monochromatic spectrum remains challenging because of the broadband characteristic of a thermal source.[37] In this work, we demonstrate an electrically driven metasurface consisting of a YUA array [Fig. 1(a)], which enables narrowband and directional thermal emission. The Wiener-chaos expansion (WCE) method combined with finite-difference time-domain simulation by ANSYS Lumerical FDTD is applied for investigating the spectral and directional performance of this metasurface. The influence of substrate on the spectral response is analyzed by an equivalent circuit model.

A YUA is composed of an actively driven element called *feed* surrounded by a *reflector* and a few *directors* as illustrated in Fig. 1(b). As a dipole resonator, the feed nanorod supports dipole-like resonance that will interact with the emission of reflector and director elements. Accordingly, the length of the feed element plays a crucial role in determining the operating frequency. Placing a longer reflector near the feed will induce inductive detuning due to its lower resonance frequency, while adding shorter directors can have a capacitive detuning effect on the whole structure.[29] Consequently, the YUA suppresses electromagnetic wave propagation in the backward direction and leads to increased directionality in the forward direction [positive x in Fig. 1(b)]. Here, gold nanorods are employed in our YUA design. At the designed emitting wavelength of 6.5 μm, we determine the dimensions of components in an individual antenna as follows:[37] the feed nanorod has a length of 2.5 μm and a cross section of $150 \times 150\,\text{nm}^2$, the reflector is 3 μm long and has a cross section of $200 \times 150\,\text{nm}^2$, and the directors are 2.2 μm long with a cross section of $100 \times 150\,\text{nm}^2$. To achieve effective constructive or destructive interference, spacings between the feed and reflector/director elements are optimized based on the maximum directivity and forward-to-backward emission intensity ratio (see supplementary material Note S1). The directivity of the antenna defined for all emission angles is expressed by

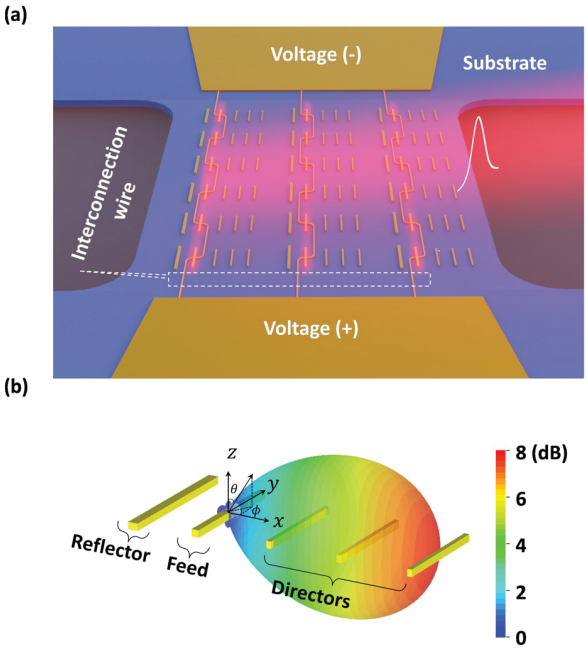

FIG. 1. (a) Schematic of an electrically driven nanoantenna metasurface achieving narrowband and directional thermal emission. (b) Schematic of a YUA with directional far-field emission profile.

$$D(\theta, \phi) = \frac{I(\theta, \phi)}{P_{tot}/4\pi}, \tag{1}$$

where θ and ϕ are the zenith and azimuth angles, respectively, in the standard spherical coordinate; $I(\theta, \phi)$ is the radiation intensity; and P_{tot} is the total emissive power. As a result, the reflector-to-feed spacing is determined to be 1.2 μm, while the separation is 1.5 μm between the feed and director as well as among neighboring directors, from which the directivity distribution is obtained in Fig. 1(b).

To characterize the narrowband and directional performance of the metasurface, we conduct the full-wave simulation by ANSYS Lumerical FDTD, in which the WCE method is used to properly excite the feed. In the WCE method,[38] thermally induced random currents are expanded into deterministic orthonormal current modes. Each current mode can be represented by a series of dipole sources in the emitting element with assigned amplitudes that satisfy the orthonormal basis function (see supplementary material Note S2 for detailed implementation of WCE). From the WCE method, the far-field spatial and spectral responses are captured by a box of monitors enclosing the whole antenna structure. In FDTD, we utilize the following built-in analysis groups to obtain spectral emissivity, far-field electric field intensity distribution, and directivity: the transmission box, the far-field from the closed box, and directivity. For a single unit, including the nanorod, YUA, and YUA with interconnection wire (wired-YUA) structures, the polar plots in Fig. 2(a) reveal the radiation patterns in the upper hemisphere as a function of polar and azimuthal angles. Without reflector and director elements, the nanorod possesses dipole-like emission. However, with the interference of reflector and directors, the emission

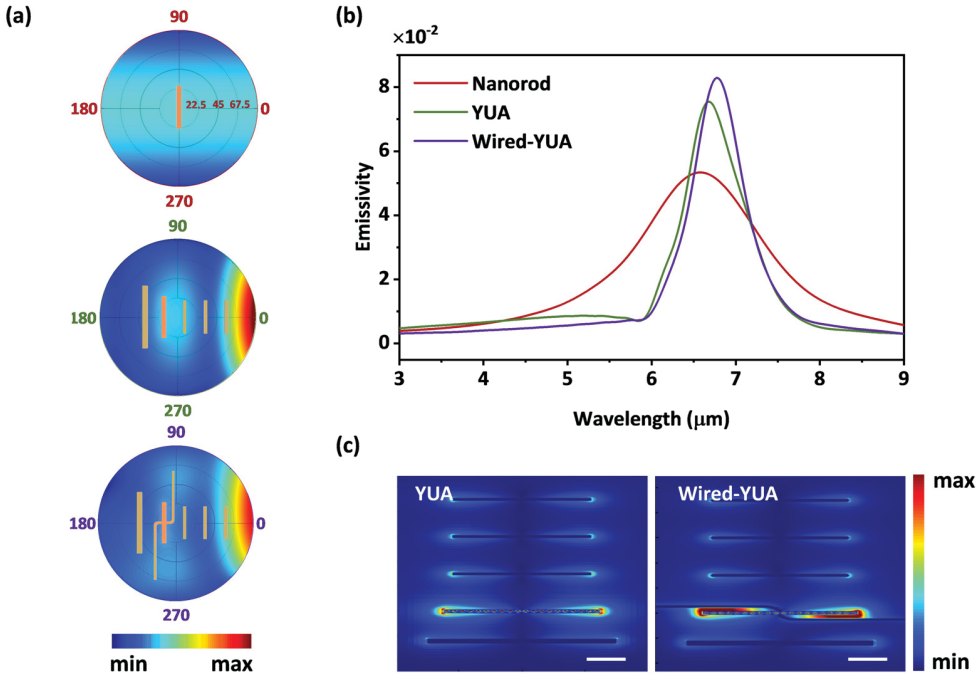

FIG. 2. (a) Far-field electric field intensity distribution of a nanorod, a YUA, and a wired-YUA at their corresponding resonant wavelengths of 6.5, 6.7, and 6.8 μm, respectively. (b) Emissivity of the nanorod, YUA, and wired-YUA. (c) Electric field profile of the YUA and wired-YUA. Scale bar: 0.6 μm.

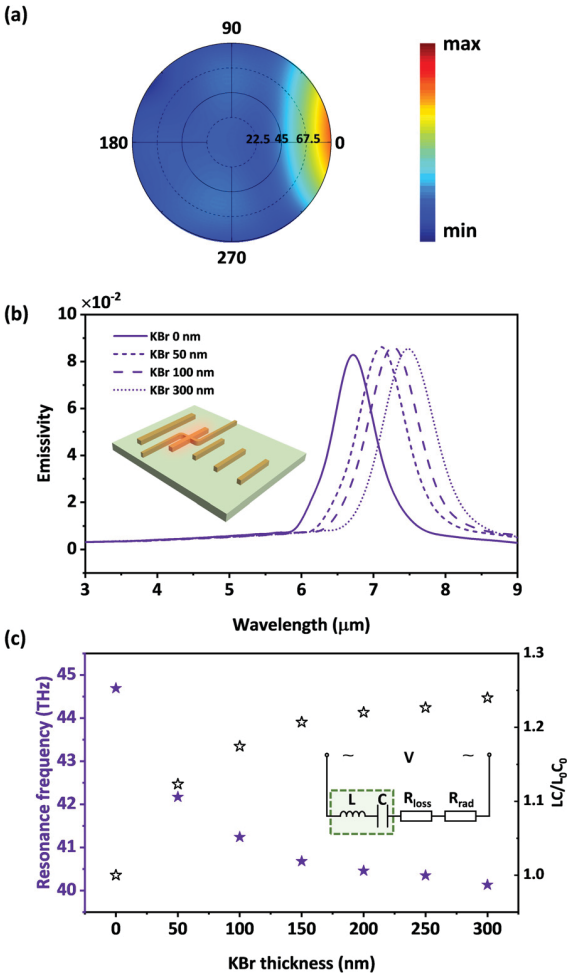

FIG. 3. (a) Far-field electric field intensity distribution of the wired-YUA with a 50 nm thick KBr substrate at the corresponding resonant wavelength of 7.1 μm. (b) Emissivity of the wired-YUA on the KBr substrates with different thicknesses. (c) Resonant frequency and corresponding normalized total LC vs substrate thickness. Inset: Equivalent circuit model of the wired-YUA with a substrate.

is strongly beamed in the forward direction and forms a narrow-angle lobe at the azimuthal angle of 0°. From the spectral perspective [Fig. 2(b)], it is evident that a gold nanorod of 2.5 μm supports the dipole-like resonance at 6.5 μm. The YUA, as a result of detuning from reflector and director elements,[35] slightly red shifts and resonates at the wavelength around 6.7 μm. Meanwhile, the temporal destructive interference at the wavelength of about 5.85 μm significantly truncates the bandwidth and leads to stronger temporally coherent emission. To activate the YUA electrically, an S-shaped interconnection wire is employed to connect the feed element. By applying a voltage bias, the interconnection electrode allows local Joule heating, which can electrothermally excite the feed. From our previous study,[24] the center-connected electrode wire shows a minimal impact on the resonator due to the wire only occupying the center of the feed where the field intensity is the weakest. However, the asymmetric S-shaped wire for a single wired-YUA here induces a minor tilt in the mainlobe direction [Fig. 2(a)]. In the metasurface structure, such a directional offset is canceled out due to the zigzag "S" feature (see following Fig. 4 and supplementary material Note S3). Furthermore, with the interconnection wire, the spectral resonance experiences a red shift to 6.8 μm [Fig. 2(b)]. This can be explained by the electric field profile shown in Fig. 2(c), where the coupling between the wire and the feed generates a slightly tilted electric distribution, corresponding to a longer effective dipole moment.

To complete the design of the *nanoantenna metasurface*, we have chosen Potassium Bromide (KBr)[39] as the substrate due to its infrared lossless, high transparency, and thermal stability. The directional emission behavior is sustained, as demonstrated by the example of 50 nm of KBr shown in Fig. 3(a). In Fig. 3(b), when the KBr substrate thickness is gradually changed from 0 to 300 nm, the resonance frequency is red shifted. It is instructive to analyze the influence of substrate thickness on the resonator behavior within an equivalent circuit model. In this case, the antenna can be described as a passive one-port circuit that presents an impedance to the electrical source. With R_{loss} representing the non-radiative loss (e.g., heat dissipation through heat conduction and natural convection) and R_{rad} as the radiative loss, the introduction of the lossless KBr substrate significantly changes the energy storage elements L, C of the antenna, as shown in Fig. 3(c) inset. To explain the shift of resonance frequency with increasing substrate thickness, a simple serial circuit analysis[40,41] can give the variation in resonant frequency as

$$\frac{LC}{L_0C_0} = \left(\frac{\omega_0}{\omega}\right)^2, \tag{2}$$

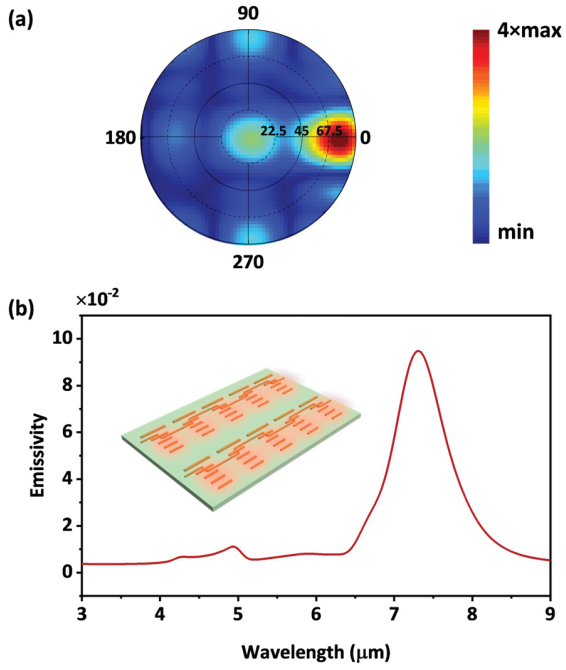

FIG. 4. (a) Far-field electric field intensity distribution of the nanoantenna array metasurface (10 units) with a 50 nm thick KBr substrate at the corresponding resonant wavelength of 7.1 μm. (b) Emissivity of the metasurface. Inset: metasurface schematic.

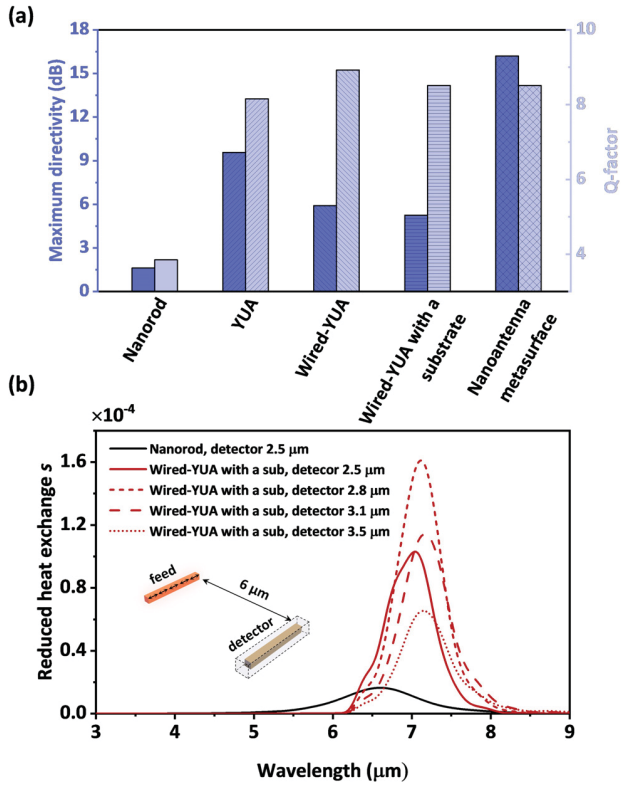

FIG. 5. (a) Maximum directivity and Q-factor of the emission from a nanorod, a YUA, a wired-YUA with/without the KBr substrate, and nanoantenna metasurface (10 units). (b) Reduced heat exchange spectra between the feed and a detector of different lengths.

where $\omega_0 = (L_0C_0)^{-1/2}$ is the limit of the resonance frequency of the wired-YUA when the substrate is absent. In Fig. 3(c), as the resonance frequency is inversely correlated with the substrate thickness, according to Eq. (2), a positive relationship between the substrate thickness and the corresponding normalized overall *LC* value is indicated. The energy stored in the capacitor and inductor is directly proportional to their respective *C* and *L* values. Consequently, an increase in the *LC* value results in a greater amount of stored energy. Therefore, a thicker KBr layer corresponds to a larger portion of the stored energy. Moreover, the introduction of the substrate can benefit a higher energy injection efficiency by matching the overall impedance to the source. In the consideration of hygroscopicity of KBr thin film,[42,43] the feasible fabrication of the metasurface can be accomplished by electron beam lithography patterning on a thick KBr substrate, following a similar approach as in our previous work.[24]

Figure 4 reveals the directional and spectral performance of the nanoantenna array metasurface of 10 units. Constructive interference among neighboring units in each row results in a much narrower lobe in the forward direction. However, the mainlobe slightly points upward (positive *z*) due to interference among different rows. Spectrally, the narrowband feature remains, with the absolute emissive power linearly proportional to the number of units in the metasurface (for more details, refer to supplementary material Note S3).

Based on all aforementioned scenarios, including nanorod, YUA, wired-YUA with/without the KBr substrate, and nanoantenna metasurface (10 units), the directional and narrowband performance, characterized by maximum directivity and Q-factor [defined by Eq. (3)], respectively, are summarized in Fig. 5(a). It is clear that the presence of reflector and director elements can significantly improve emissive directionality, leading to a concentration of radiative energy. Although the presence of S-shaped wire slightly deteriorates the directionality, the constructive interference in the array configuration enhances the beaming effect drastically. For example, with a metasurface consisting of 10 units, it demonstrates approximately one order of magnitude higher directivity compared to a single nanorod. Furthermore, the Q-factor is substantially enhanced as compared to a dipole resonator,

$$Q = \frac{\lambda_{res}}{\Delta\lambda_{FWHM}}. \tag{3}$$

Finally, to quantify the enhancement of the forward emissive power, a nanorod detector is placed 6 μm away from the feed along the *x* axis. By appropriate detector configuration as shown in Fig. 5(b) (see supplementary material Note S2 for details), we obtain the reduced heat exchange between the emitting feed and receiving detector *s*, which relates to the total heat transfer by

$$P = \int s(\Theta(\omega, T_1) - \Theta(\omega, T_2))d\omega, \tag{4}$$

where $\Theta(\omega, T)$ is the Plank distribution defined by $\hbar\omega/\left[\exp\left(\frac{\hbar\omega}{k_BT}\right) - 1\right]$ and T_1 and T_2 are the feed and detector temperatures, respectively. It is apparent from Fig. 5(b) that compared to a nanorod resonator, the wired-YUA with the KBr substrate (when KBr is 50 nm thick) can greatly improve the receiving energy by approximately one order of magnitude at the spectral peak when the detector shares the identical geometry with the feed. It is worth noting that the length of the detector affects the radiative heat exchange. Since the wired-YUA with a substrate resonates at a longer wavelength than the intrinsic resonance of the feed, a longer detector (2.8 μm) can better couple with the resonance from the emitting YUA and boost heat transfer. However, if the detector is further elongated (e.g., 3.5 μm), it will lead to resonance mismatch and decrease radiative heat transfer.

In summary, this study presents a nanoantenna metasurface design that achieves highly directional and narrowband thermal emission in the mid-infrared range. The use of the S-shaped interconnection wire further allows electrical excitation while maintaining the high directionality. The WCE method implemented by the FDTD platform is established to investigate spectral and directional performance of the metasurface. The influence of a transparent substrate on the overall spectral response is analyzed by an equivalent circuit model. In comparison with a single nanorod, the coherence of the thermal emission from the metasurface (10 units) is greatly improved, leading to one order of magnitude enhancement in the directivity and several times improvement in the Q-factor. This work introduces a promising approach for directional narrowband thermal emission control, which has important implications in the fields of infrared imaging, sensing, and energy harvesting.

See the supplementary material for supplementary Notes S1–S3 and Figs. S1–S3.

The authors thank Zhuo Li for his valuable comments on this work. The authors are grateful to the Defense Threat Reduction Agency (Grant No. HDTRA1-19-1-0028) and the National Science Foundation (Grant No. CBET-1931964).

AUTHOR DECLARATIONS

Conflict of Interest

The authors have no conflicts to disclose.

Author Contributions

Lin Jing and Xiu Liu contributed equally to this work.

Lin Jing: Conceptualization (lead); Formal analysis (lead); Investigation (equal); Methodology (equal); Validation (equal); Visualization (equal); Writing – original draft (equal). **Xiu Liu:** Conceptualization (equal); Formal analysis (lead); Investigation (equal); Methodology (equal); Validation (equal); Writing – original draft (equal). **Hakan Salihoglu:** Formal analysis (equal); Investigation (equal); Validation (equal); Writing – review & editing (equal). **Xiao Luo:** Formal analysis (equal); Investigation (equal); Validation (equal); Writing – review & editing (equal). **Hyeong Seok Yun:** Formal analysis (equal); Investigation (equal); Validation (equal); Writing – review & editing (equal). **Zexiao Wang:** Formal analysis (equal); Visualization (equal); Writing – review & editing (equal). **Sheng Shen:** Supervision (lead); Writing – review & editing (equal).

DATA AVAILABILITY

The data that support the findings of this study are available from the corresponding author upon reasonable request.

REFERENCES

[1]A. Tittl, A.-K. U. Michel, M. Schäferling, X. Yin, B. Gholipour, L. Cui, M. Wuttig, T. Taubner, F. Neubrech, and H. Giessen, "A switchable mid-infrared plasmonic perfect absorber with multispectral thermal imaging capability," Adv. Mater. **27**, 4597 (2015).
[2]J. Feng, V. S. Siu, A. Roelke, V. Mehta, S. Y. Rhieu, G. T. R. Palmore, and D. Pacifici, "Nanoscale plasmonic interferometers for multispectral, high-throughput biochemical sensing," Nano Lett. **12**, 602 (2012).
[3]H. T. Miyazaki, T. Kasaya, M. Iwanaga, B. Choi, Y. Sugimoto, and K. Sakoda, "Dual-band infrared metasurface thermal emitter for CO_2 sensing," Appl. Phys. Lett. **105**, 121107 (2014).
[4]A. P. Raman, M. A. Anoma, L. Zhu, E. Rephaeli, and S. Fan, "Passive radiative cooling below ambient air temperature under direct sunlight," Nature **515**, 540 (2014).
[5]R. Scheibner, M. König, D. Reuter, A. D. Wieck, C. Gould, H. Buhmann, and L. W. Molenkamp, "Quantum dot as thermal rectifier," New J. Phys. **10**, 083016 (2008).
[6]A. Lenert, D. M. Bierman, Y. Nam, W. R. Chan, I. Celanović, M. Soljačić, and E. N. Wang, "A nanophotonic solar thermophotovoltaic device," Nat. Nanotechnol. **9**, 126 (2014).
[7]D. M. Bierman, A. Lenert, W. R. Chan, B. Bhatia, I. Celanović, M. Soljačić, and E. N. Wang, "Enhanced photovoltaic energy conversion using thermally based spectral shaping," Nat. Energy **1**, 16068 (2016).
[8]A. Lochbaum, Y. Fedoryshyn, A. Dorodnyy, U. Koch, C. Hafner, and J. Leuthold, "On-chip narrowband thermal emitter for mid-IR optical gas sensing," ACS Photonics **4**, 1371 (2017).
[9]W. Li and S. Fan, "Nanophotonic control of thermal radiation for energy applications [Invited]," Opt. Express **26**, 15995 (2018).
[10]Y. Li, W. Li, T. Han, X. Zheng, J. Li, B. Li, S. Fan, and C.-W. Qiu, "Transforming heat transfer with thermal metamaterials and devices," Nat. Rev. Mater. **6**, 488 (2021).
[11]S. Campione, F. Marquier, J.-P. Hugonin, A. R. Ellis, J. F. Klem, M. B. Sinclair, and T. S. Luk, "Directional and monochromatic thermal emitter from epsilon-near-zero conditions in semiconductor hyperbolic metamaterials," Sci. Rep. **6**, 34746 (2016).
[12]M. C. Larciprete, M. Centini, R. Li Voti, and C. Sibilia, "Asymmetric and tunable infrared emission in metamaterials composed by oriented air voids into a polar material," J. Mod. Opt. **66**, 299 (2019).
[13]Y. Zhang, M. Antezza, H.-L. Yi, and H.-P. Tan, "Metasurface-mediated anisotropic radiative heat transfer between nanoparticles," Phys. Rev. B **100**, 085426 (2019).
[14]C. Simovski, S. Maslovski, I. Nefedov, and S. Tretyakov, "Optimization of radiative heat transfer in hyperbolic metamaterials for thermophotovoltaic applications," Opt. Express **21**, 14988 (2013).
[15]B. Liu, W. Gong, B. Yu, P. Li, and S. Shen, "Perfect thermal emission by nanoscale transmission line resonators," Nano Lett. **17**, 666 (2017).
[16]X. Liu, T. Tyler, T. Starr, A. F. Starr, N. M. Jokerst, and W. J. Padilla, "Taming the blackbody with infrared metamaterials as selective thermal emitters," Phys. Rev. Lett. **107**, 045901 (2011).
[17]J. Li, Z. Li, X. Liu, S. Maslovski, and S. Shen, "Active control of thermal emission by graphene-nanowire coupled plasmonic metasurfaces," Phys. Rev. B **106**, 115416 (2022).
[18]B. Liu, J. Li, and S. Shen, "Resonant thermal infrared emitters in near- and far-fields," ACS Photonics **4**, 1552 (2017).
[19]J.-J. Greffet, R. Carminati, K. Joulain, J.-P. Mulet, S. Mainguy, and Y. Chen, "Coherent emission of light by thermal sources," Nature **416**, 61 (2002).
[20]N. Dahan, A. Niv, G. Biener, Y. Gorodetski, V. Kleiner, and E. Hasman, "Enhanced coherency of thermal emission: beyond the limitation imposed by delocalized surface waves," Phys. Rev. B **76**, 045427 (2007).
[21]M. Makhsiyan, P. Bouchon, J. Jaeck, J.-L. Pelouard, and R. Haïdar, "Shaping the spatial and spectral emissivity at the diffraction limit," Appl. Phys. Lett. **107**, 251103 (2015).
[22]F. Marquier, K. Joulain, J.-P. Mulet, R. Carminati, J.-J. Greffet, and Y. Chen, "Coherent spontaneous emission of light by thermal sources," Phys. Rev. B **69**, 155412 (2004).
[23]X. Liu, Z. Li, Z. Wang, H. S. Yun, and S. Shen, "Design and analysis of electro-thermal metasurfaces," Front. Energy **17**, 134 (2023).
[24]X. Liu, L. Jing, X. Luo, B. Yu, S. Du, Z. Wang, H. Kim, Y. Zhong, and S. Shen, "Electrically driven thermal infrared metasurface with narrowband emission," Appl. Phys. Lett. **121**, 131703 (2022).
[25]D. Costantini, A. Lefebvre, A.-L. Coutrot, I. Moldovan-Doyen, J.-P. Hugonin, S. Boutami, F. Marquier, H. Benisty, and J.-J. Greffet, "Plasmonic metasurface for directional and frequency-selective thermal emission," Phys. Rev. Appl. **4**, 014023 (2015).
[26]M. Centini, M. C. Larciprete, R. L. Voti, M. Bertolotti, C. Sibilia, and M. Antezza, "Hybrid thermal Yagi-Uda nanoantennas for directional and narrow band long-wavelength IR radiation sources," Opt. Express **28**, 19334 (2020).
[27]C. A. Balanis, "Antenna theory: A review," Proc. IEEE **80**, 7 (1992).
[28]L. C. Godara, "Application of antenna arrays to mobile communications, Part II: Beam-forming and direction-of-arrival considerations," Proc. IEEE **85**, 1195 (1997).
[29]H. F. Hofmann, T. Kosako, and Y. Kadoya, "Design parameters for a nano-optical Yagi–Uda antenna," New J. Phys. **9**, 217 (2007).
[30]I. S. Maksymov, I. Staude, A. E. Miroshnichenko, and Y. S. Kivshar, "Optical Yagi-Uda nanoantennas," Nanophotonics **1**, 65 (2012).
[31]H. Galal and M. Agio, "Highly efficient light extraction and directional emission from large refractive-index materials with a planar Yagi-Uda antenna," Opt. Mater. Express **7**, 1634 (2017).
[32]A. G. Curto, G. Volpe, T. H. Taminiau, M. P. Kreuzer, R. Quidant, and N. F. van Hulst, "Unidirectional emission of a quantum dot coupled to a nanoantenna," Science **329**, 930 (2010).
[33]D. Dregely, R. Taubert, J. Dorfmüller, R. Vogelgesang, K. Kern, and H. Giessen, "3D optical Yagi–Uda nanoantenna array," Nat. Commun. **2**, 267 (2011).
[34]J. Ho, Y. H. Fu, Z. Dong, R. Paniagua-Dominguez, E. H. H. Koay, Y. F. Yu, V. Valuckas, A. I. Kuznetsov, and J. K. W. Yang, "Highly directive hybrid metal–dielectric Yagi-Uda nanoantennas," ACS Nano **12**, 8616 (2018).
[35]T. Kosako, Y. Kadoya, and H. F. Hofmann, "Directional control of light by a nano-optical Yagi–Uda antenna," Nat. Photonics **4**, 312 (2010).
[36]R. Kullock, M. Ochs, P. Grimm, M. Emmerling, and B. Hecht, "Electrically-driven Yagi-Uda antennas for light," Nat. Commun. **11**, 115 (2020).

[37]B. Yu, J. Li, and S. Shen, "Directional control of narrow-band thermal emission from nanoantennas," J. Photonics Energy **9**, 032712 (2019).
[38]Z. Li, J. Li, X. Liu, H. Salihoglu, and S. Shen, "Wiener Chaos expansion method for thermal radiation from inhomogeneous structures," Phys. Rev. B **104**, 195426 (2021).
[39]H. H. Li, "Refractive index of alkali halides and its wavelength and temperature derivatives," J. Phys. Chem. Ref. Data **5**, 329 (1976).
[40]T. Driscoll, H.-T. Kim, B.-G. Chae, B.-J. Kim, Y.-W. Lee, N. M. Jokerst, S. Palit, D. R. Smith, M. Di Ventra, and D. N. Basov, "Memory metamaterials," Science **325**, 1518 (2009).
[41]A. Dorodnyy, S. M. Koepfli, A. Lochbaum, and J. Leuthold, "Design of CMOS-compatible metal–insulator–metal metasurfaces via extended equivalent-circuit analysis," Sci. Rep. **10**, 17941 (2020).
[42]R. Z. Zhang and K. Araki, "Ultralow emittance thermal radiation barrier achieved by a high-contrast grating coating," J. Thermophys. Heat Transfer **37**, 227 (2023).
[43]M. A. Blankenship, K. D. Adams, and R. Z. Zhang, "Gradient-index metasurface multilayer for quasioptical coupling of infrared detectors," Opt. Eng. **60**, 107102 (2021).